Published in final edited form as:
Cancer Cell. 2014 January 13; 25(1): 21–36. doi:10.1016/j.ccr.2013.12.007.

CARM1 Methylates Chromatin Remodeling Factor BAF155 to Enhance Tumor Progression and Metastasis

Lu Wang[1], **Zibo Zhao**[1], **Mark B. Meyer**[2], **Sandeep Saha**[3], **Menggang Yu**[3], **Ailan Guo**[4], **Kari B. Wisinski**[5], **Wei Huang**[6], **Weibo Cai**[7], **J. Wesley Pike**[2], **Ming Yuan**[8,9], **Paul Ahlquist**[1,8,10], and **Wei Xu**[1,*]

[1]McArdle Laboratory for Cancer Research, University of Wisconsin-Madison, Madison, WI 53706, USA

[2]Department of Biochemistry, University of Wisconsin-Madison, Madison, WI 53706, USA

[3]Department of Biostatistics and Medical Informatics, University of Wisconsin-Madison, Madison, WI 53706, USA

[4]Cell Signaling Technology, Danvers, MA 01923, USA

[5]Department of Medicine, University of Wisconsin-Madison, Madison, WI 53706, USA

[6]Department of Pathology, University of Wisconsin-Madison, Madison, WI 53706, USA

[7]Department of Radiology, University of Wisconsin-Madison, Madison, WI 53706, USA

[8]Morgridge Institute for Research, University of Wisconsin-Madison, Madison, WI 53706, USA

[9]Department of Statistics, University of Wisconsin-Madison, Madison, WI 53706, USA

[10]Howard Hughes Medical Institute, University of Wisconsin-Madison, Madison, WI 53706, USA

Summary

Coactivator-associated arginine methyltransferase 1 (CARM1), a coactivator for various cancer-relevant transcription factors, is overexpressed in breast cancer. To elucidate the functions of CARM1 in tumorigenesis, we knocked out *CARM1* from several breast cancer cell lines using Zinc-Finger Nuclease technology, which resulted in drastic phenotypic and biochemical changes. The *CARM1* KO cell lines enabled identification of CARM1 substrates, notably the SWI/SNF core subunit BAF155. Methylation of BAF155 at R1064 was found to be an independent prognostic biomarker for cancer recurrence and to regulate breast cancer cell migration and metastasis. Furthermore, CARM1-mediated BAF155 methylation affects gene expression by directing methylated BAF155 to unique chromatin regions (e.g., c-Myc pathway genes). Collectively, our studies uncover a mechanism by which BAF155 acquires tumorigenic functions via arginine methylation.

*Correspondence: wxu@oncology.wisc.edu.

Accession Numbers: The ChIP-seq data are available at the Gene Expression Omnibus under the accession number GSE52964.

Supplemental Information: Supplemental Information includes Supplemental Experimental Procedures, seven figures, and three tables and can be found with this article online at http://dx.doi.org/10.1016/j.ccr.2013.12.007.

Introduction

Coactivator-associated arginine methyltransferase 1 (CARM1), also known as PRMT4, is a type I protein arginine methyltransferase (PRMT) that asymmetrically dimethylates protein substrates on arginine residues. CARM1 was originally identified as a coactivator for steroid hormone receptors (Chen et al., 1999). CARM1 knockout (KO) mice die at birth (Yadav et al., 2003), showing that CARM1 is specifically required for postnatal survival. Interestingly, methyltranserase-inactivated *CARM1* knockin mice phenocopy CARM1 null mice, indicating that CARM1 requires its enzymatic activity for the majority, if not all, of its in vivo functions (Kim et al., 2010).

Emerging evidence implies oncogenic functions of CARM1 in human cancer. CARM1 transactivates many cancer-associated transcription factors including NF-κB, p53, E2F1, and steroid receptors such as estrogen receptor alpha (ERα; Bedford and Clarke, 2009), and promotes cancer cell proliferation (El Messaoudi et al., 2006; Frietze et al., 2008). Recent tissue microarray studies revealed that CARM1 expression is higher in metastatic breast tumors than in normal breast tissues (Mann et al., 2013), particularly in triple negative tumors lacking expression of ERα, PR, and HER2 (Davis et al., 2013). These results imply that altered CARM1expression may underlie pathological conditions and that, in breast cancer, CARM1 has roles beyond serving as a coactivator for ERα. It remains to be determined whether the oncogenic functions of CARM1 depend on its ability to regulate cancer-driving transcription factors or to directly methylate cancer-relevant substrates, or both.

The significance of identifying cancer-relevant CARM1 substrates is underscored by studies of the roles of histone H3 methylation in transcriptional activation of ER target genes (Wu and Xu, 2012). Nonhistone substrates include p300/CBP, AIB1/SRC-3, and RNA binding proteins such as PABP1, HuR, HuD, and HnRNPs (Bedford and Clarke, 2009). Multiple lines of evidence indicate that normal CARM1 expression is well above that required for its essential roles. For instance, normal developmental functions were maintained in genetically engineered *CARM1* hypomorphic mice with only 25% of the wild-type (WT) *CARM1* level (Kim et al., 2010). We recently showed that knocking down 90% of endogenous CARM1 in MCF7 cells only slightly reduces methylation of PABP1 (Zeng et al., 2013). These results imply that even greatly depleted CARM1 catalytic activity and substrate methylation are sufficient to maintain major biological functions. Previously, CARM1 null mouse embryonic fibroblast cell lysates were used as a hypomethylated substrate source that led to identifying PABP1 as a CARM1 substrate (Lee and Bedford, 2002). The CARM1 null cancer cell lines would greatly facilitate identifying cancer-relevant substrates and understanding of CARM1 oncogenic functions in breast cancer cells. Herein, we generated *CARM1* KO cancer cell lines and used them to explore the roles of BAF155 methylation by CARM1 in breast cancer models.

Results

Generation of *CARM1* KO Breast Cancer Cell Lines Using ZFN Technology

We recently developed a sensitive methylated PABP1 (me-PABP1) western blot method to monitor endogenous CARM1 levels and activity (Zeng et al., 2013). In contrast to the complete loss of me-PABP1 in *CARM1* null mouse embryonic fibroblasts (*CARM1*$^{-/-}$ MEFs; Figure 1A, lanes 1 and 2), we found that even though small hairpin RNA (shRNA)-mediated knockdown decreased CARM1 levels by 90%, the cellular me-PABP1 level decreased by less than 20% (Figure 1A, lanes 3 and 4). Thus, low levels of CARM1 are capable of substantial PABP1 methylation. Because CARM1 substrates therefore should remain significantly methylated in *CARM1* knockdown cells but be hypomethylated in *CARM1* null cells, we generated *CARM1* null cancer cell lines to identify cancer-relevant CARM1 substrates. We utilized Zinc Finger Nuclease (ZFN) technology to create a highly specific genomic scissors targeting exon 8 of *CARM1* (Figure 1B), and through this generated a complete KO in cancer cell lines. After transient transfection of ZFN plasmids into cells, we performed limiting dilution to select single clones and confirmed *CARM1* KO by loss of me-PABP1 (Figure 1C) and genomic DNA sequencing (Figure 1D). Representative KO clones with complete depletion of me-PABP1 are shown in Figure 1C for MCF7, MDA-MB-231, and human embryonic kidney 293T (HEK293T) cell lines. The human *CARM1* gene locus resides at chromosome19 p13.2, a region triplicated in MCF7 and duplicated in MDA-MB-231 cells. The genomic DNA sequencing analysis of two representative CARM1 KO clones of MCF7 and MDA-MB-231 (Figure 1D) revealed misrepaired DNA, resulting in mRNA degradation and gene deletion. Although the efficiency of ZFN KO varied among cell lines at 1.3%, 0.5%, and 3.6% for MCF7, MDA-MB-231, and HEK293T, respectively, the average KO efficiency across all clones analyzed was 1.2% (Figure 1E). When CARM1 was re-expressed in two individual MCF7 *CARM1* KO clones, me-PABP1 was restored (Figure 1F). Interestingly, we found that KO of *CARM1* in MCF7 cells induced morphology changes (Figure 1G), whereas no morphology change was observed in MCF7 cells expressing CARM1 shRNA to knock down CARM1 to 10% of WT levels (Figure 1G). The morphology change in the two KO clones was rescued by re-expressing WT CARM1 (Figure 1G) but not an enzyme-defective mutant (data not shown). We compared the in vitro cell growth and in vivo tumor growth of MDA-MB-231 *CARM1* KO and MCF7 *CARM1* KO with their parental cells. KO of CARM1 impeded cell growth and colony formation (Figures S1A and S1B available online) and tumor growth in vivo (Figure S1C). These data strongly suggest that the cell morphology change and growth defect in KO cells could be due to loss of methylation of CARM1 substrates.

Identification of BAF155 as a Substrate for CARM1

The lack of understanding of the biological functions of CARM1 in cancers is at least partially attributed to the limited number of known CARM1 substrates. A few CARM1 substrates were previously identified or validated by comparing *CARM1*$^{+/+}$ and *CARM1*$^{-/-}$ MEF cell lysates for in vitro and in vivo methylation (Cheng et al., 2007; Kim et al., 2004). In contrast to CARM1-expressing cells, where potential CARM1 substrates would be blocked for further methylation, *CARM1*$^{-/-}$ MEF lysates served as a hypomethylated substrate resource for CARM1 substrate identification. Indeed, we found that MCF7

CARM1 KO cell lysates were more strongly methylated in vitro by recombinant CARM1 protein than *CARM1*$^{-/-}$ MEF cell lysates, as assayed by $^{3}H\text{-}CH_3$ labeling in an autoradiograph (Figure S2A) and western blotting using a newly developed asymmetrically dimethylated arginine (α-ADMA) antibody (Dhar et al., 2013; Figure S2B). This result implies that MCF7 *CARM1* KO cells serve as a good resource for substrate discovery.

When cell lysates derived from parental MCF7 cells and *CARM1* KO cells were probed with monomethylated arginine (α-MMA) and α-ADMA antibodies in western blots, asymmetrically dimethylated proteins, in particular those in the high molecular weight range, were significantly affected by *CARM1* KO (Figure 2A). This is in contrast to the lack of a significant effect on monomethylated proteins. In order to identify CARM1 substrates in breast cancer cells, we used the α-ADMA antibody to immunoprecipitate proteins from cell lysates derived from parental MCF7 cells expressing WT CARM1 and MCF7 CARM1 KO cells, respectively. The discrete bands in WT cells stained with Coomassie blue were excised and subjected to mass spectrometry, from which ten candidate proteins were identified (Figure 2B). To discern whether these proteins are CARM1 substrates, we immunoprecipitated endogenous proteins (BRG1, BAF170, BAF155, and BAF250) or FLAG-tagged proteins (TRAP150, Caprin 1, TRAP230, and BCLAF1) transiently transfected to MCF7 WT or KO cells, and followed their fate in western blots using α-ADMA or α-FLAG antibody, respectively.

Western blot results using α-ADMA antibody (Figure 2C) classified the candidate proteins into three categories. The first category includes BAF155 and TRAP230 proteins, which are dimethylated in WT but not in KO MCF7 cells, indicating that arginine dimethylation of these proteins is CARM1 dependent. The second category includes Caprin1 and BCLAF1 proteins, which are dimethylated in WT and KO cells at similar levels, indicating that CARM1 is not their sole methyltransferase. Finally, the third category includes BAF170, BRG1, BAF250, and TRAP150 proteins, which are not recognized by α-ADMA antibody, suggesting that they were immunoprecipitated by the α-ADMA antibody via indirect association with bone fide CARM1 substrates (e.g., BRG1, BAF250, and BAF170 are in complex with methylated BAF155). Although the α-ADMA antibody recently developed by Cell Signaling appeared sensitive in detecting CARM1 substrates, this antibody has not been extensively characterized (Dhar et al., 2013).

Since a previous study had reported that a histone H3 arginine17 dimethylation (H3R17me2) antibody, while recognizing the H3R17me2 mark, also recognized other CARM1 substrates in MEF cells (Cheng et al., 2007), we employed this anti-H3R17me2 antibody for western blotting (Figure S2C, left panel) and immunoprecipitation, followed by Coomassie blue staining (Figure S2C, right panel), using total cell lysates from MCF7 WT and KO cells. Similar to the pattern detected by α-ADMA antibody, the recognized proteins specific to *CARM1* WT but not *CARM1* KO cells reside in the high molecular weight range, among which BAF155 was identified using mass spectrometry (Figure S2C). Correspondingly, one strong band (Figure S2D, arrow head) migrating between 130 and 250 kDa was detected by α-ADMA antibody in the α-H3R17me2 immunoprecipitates from WT but not KO MCF7 cell lysates. This band was subsequently proved to be BAF155 by reciprocal immunoprecipitation using H3R17me2 and BAF155 antibodies (Figures S2E and

S2F). Collectively, BAF155 appeared to be a main substrate of CARM1 in MCF7 cells detected by both α-ADMA and H3R17me2 antibodies.

To address whether BAF155is methylated by CARM1 directly, we performed in vitro methylation assays using recombinant CARM1 and hypomethylated BAF155 purified from HEK293T CARM1 KO cells in the presence of adenosyl-L-methionine, S-[methyl-^{3}H] (^{3}H-SAM). As expected, BAF155 was methylated by CARM1 in vitro (Figure 2D). Finally, we demonstrated that BAF155 methylation could be restored in HEK293T *CARM1* KO cells by expressing WT CARM1 but not a methylation-defective mutant (Figure 2E). These results collectively demonstrate that CARM1 is both necessary and sufficient to methylate BAF155. In keeping with this finding, CARM1 was found to be the only PRMT among PRMT family members (PRMT1–PRMT8) that is capable of methylating BAF155 in vitro (Figure S2G).

CARM1 Methylates BAF155 at a Single Site, R1064

Although multiple CARM1 substrates were discovered using the α-ADMA antibody and CARM1 KO cell line (Figure 2B), we chose to focus on BAF155 because BAF155, a core subunit of switch/sucrose nonfermentable (SWI/SNF) chromatin remodeling complex, has been reported upregulated in colon, cervical, and prostate cancer (Lapointe et al., 2004; Tomlins et al., 2007; Varambally et al., 2005). Using PMeS (Shi et al., 2012), an online tool for predicting protein methylation sites based on an enhanced feature-encoding scheme, five putative arginine methylation sites were predicted on human BAF155 (Table S1). Based on the putative methylation sites, a full-length and four C-terminally truncated BAF155 derivatives with C-terminal myc tags were constructed (Figure 3A). These plasmids were transiently transfected into HEK293T cells, and the resulting proteins were immunoprecipated using α-myc antibody and western blotted with α-ADMA antibody (Figure 3B). Notably, full-length BAF155 but none of the truncated BAF155 proteins was detected by α-ADMA antibody, suggesting that the BAF155 methylation site follows residue 956. We then individually mutated C-proximal R1032 and R1064 to lysine in FLAG-tagged expression plasmids. After transient expression and anti-FLAG immunoprecipitation, FLAG-BAF155^{R1032K} but not FLAG-BAF155^{R1064K} protein was detected by α-ADMA antibody in vivo (Figure 3C). Similarly, the recombinant BAF155^{R1064K} mutant protein was not methylated by recombinant CARM1 in vitro (Figure 3D). Thus, R1064 is the only BAF155 site methylated by CARM1.

Antibodies against endogenous CARM1 or BAF155 each immunoprecipitated both proteins from MCF7 cell lysates (Figure 3E), suggesting that CARM1 and BAF155 may directly interact. To map the BAF155 region mediating association with CARM1, we linked each of a series of BAF155 truncation derivatives (Chen and Archer, 2005) with a T7 promoter and FLAG tag (Figure 3F) for in vitro transcription/translation assays. As shown in Figure 3F, full-length BAF155 and its C-terminally truncated (Δ1, Δ2, Δ3 and Δ4) but not N-terminally truncated (Δ5, Δ6 and Δ7) derivatives bound strongly to bacterially expressed glutathione S-transferase CARM1 (GST-CARM1). Thus, the acidic domain at the BAF155 N terminus mediates interaction with CARM1, although R1064, the site of methylation, localizes to the BAF155 C terminus. R1064 of human BAF155, located in the evolutionarily conserved

proline- and glutamine-rich (P/Q-rich) domain, is conserved among higher eukaryotes (Figure 3G). BAF170, while sharing 61.7% protein sequence identity with BAF155, lacks an arginine residue at a position equivalent to R1064 in its corresponding P/Q-rich domain (Figure 3H). This explains why BAF170, a close homolog of BAF155, is not a substrate for CARM1 (Figure 2C).

The Majority of Endogenous BAF155 in MCF7 Cells Is Dimethylated

To investigate the prevalence of endogenous BAF155 dimethylation in breast cancer cells, we generated a rabbit polyclonal antibody specific for dimethylated BAF155 (Figure S3A). This me-BAF155 antibody detects methylation of endogenous BAF155 in WT MCF7 cells but not in two MCF7 *CARM1* KO clones (Figure S3B). Similar to PABP1 (Figure 1A), me-BAF155 was still detectable in MCF7-sh*CARM1* cells (Figure S3C). To determine the percentage of endogenous BAF155 methylated by CARM1 in breast cancer cells, we immunoprecipitated BAF155 using the me-BAF155 antibody and performed quantitative western blotting of equal portions of the input and flow-through fractions using the total BAF155 antibody (Figure S3D). Quantitation of the band intensities across three independent experiments revealed that ~74% of endogenous BAF155 was methylated by CARM1 in MCF7 cells. Moreover, BAF155 and me-BAF155 immunofluorescence were confined to the nucleus (Figure S3E). Since the majority of endogenous BAF155 is dimethylated, we went on to study the role of BAF155 methylation in human breast cancer cells.

BAF155 Methylation at R1064 Creates Unique Chromatin Association Patterns

BAF155, a core component of the SWI/SNF chromatin remodeling complex, was shown to associate with chromatin dependently or independently of other SWI/SNF subunits using chromatin immunoprecipitation sequencing (ChIP-seq) in HeLa cells (Euskirchen et al., 2011). Accordingly, we decided to determine the effect of BAF155 methylation on its chromatin association. First, to substitute endogenous BAF155 with $BAF155^{R1064K}$ mutant, we infected MCF7 cells with retrovirus vectors expressing either WT BAF155 ($BAF155^{WT}$), mutant $BAF155^{R1064K}$, or GFP as a negative control (Figure 4A). After confirming that the resulting total BAF155 level was twice the endogenous BAF155 level, we stably knocked down endogenous BAF155 using a lentiviral-expressing shRNA, which selectively targets the 3'UTR of the endogenous, but not the lentiviral-expressed, BAF155 mRNA. Figure 4A shows that BAF155 was silenced in MCF7-GFP cells, and that MCF7-$BAF155^{WT}$ and MCF7-$BAF155^{R1064K}$ cells express reconstituted $BAF155^{WT}$ and $BAF155^{R1064K}$ proteins to levels similar to that of endogenous BAF155 protein in the parental MCF7 cells. Interestingly, substituting endogenous BAF155 with $BAF155^{R1064K}$, like *BAF155* knockdown, significantly reduced colony size (Figure 4B, lower panels) and yield (Figure 4C), while cell morphology was not changed (Figure 4B, upper panels). To investigate whether BAF155 methylation by CARM1 is required for CARM1-induced colony formation in MCF7 cells, we first stably overexpressed $BAF155^{WT}$ and $BAF155^{R1064}$ in MCF7 *CARM1* KO cells, respectively, followed by knocking down the endogenous BAF155 in these cells using lentivirus-expressing sh*BAF155*. Subsequently CARM1 was restored in MCF7 *CARM1* KO cells expressing either $BAF155^{WT}$ or $BAF155^{R1064}$, and colony formation assays were performed. The expected levels of total

BAF155, me-BAF155, and CARM1 proteins were confirmed by western blotting (Figure 4D). Restoring CARM1 in $BAF155^{WT}$-expressing but not $BAF155^{R1064K}$-expressing cells rescued colony formation in terms of both colony size and yield (Figures 4E and 4F). These results further support that BAF155 methylation affects the cellular functions of BAF155.

To ensure that BAF155 methylation does not affect its assembly into the SWI/SNF complex, we expressed $BAF155^{WT}$ and $BAF155^{R1064K}$ in SKOV3, an ovarian cancer cell line that expresses all SWI/SNF components except *BAF155* (DelBove et al., 2011). As shown in Figure S4, immunoprecipitating either $BAF155^{WT}$ or $BAF155^{R1064K}$ effectively pulled down other SWI/SNF components such as BRG1, BAF60a, and BAF47 in SKOV3 cells. Only $BAF155^{WT}$, but not $BAF155^{R1064K}$, was methylated by endogenous CARM1, as revealed by α-ADMA immunoblot (Figure S4A). Thus, both CARM1-methylated and -unmethylated BAF155 assemble into SWI/SNF complexes.

Next we determined whether methylation of BAF155 affects its chromatin association, using a genomic ChIP-seq approach with MCF7-$BAF155^{WT}$ and MCF7-$BAF155^{R1064K}$ cells. A ChIP-grade BAF155 antibody (Euskirchen et al., 2011) was used for ChIP followed by Illumina high-throughput sequencing. Representative $BAF155^{WT}$, $BAF155^{R1064K}$, and BRG1 binding sites in HeLa and MCF7 cells in a 7.5 Mb region of chromosome 8 are shown in Figure 4G. As expected, while some $BAF155^{WT}$ peaks identified in MCF7 cells overlap with the binding sites of BAF155 and BRG1 in HeLa cells (Figure 4G, box a; Euskirchen et al., 2011), $BAF155^{WT}$ also has unique binding sites in MCF7 and HeLa cells (Figure 4G, box d). We subsequently analyzed the genome-wide distribution of BAF155 binding peaks in MCF7 expressing WT or mutant BAF155. Totals of 2,667 and 1,566 peaks were identified for $BAF155^{WT}$ or $BAF155^{R1064K}$, respectively. Among these, 983 peaks overlapped (Table S2). The numbers of annotated genes in the genomic regions associated with these $BAF155^{WT}$ and $BAF155^{R1064K}$ binding sites are shown in Figure 4H. As in HeLa cells, approximately 60% of BAF155 binding sites in MCF7 cells reside in gene bodies (exons and introns; Figure 4I). Moreover, BAF155 peaks in MCF7 cells are enriched within +50 kb from the transcription starting sites (TSSs), which are likely to contain enhancer regions (Figure 4J). This pattern is consistent with those of BAF155 and BRG1, SNF5/BAF47 in HeLa cells, but it differs from those of RNA pol II, which peaks near TSSs, and BAF170, which peaks around −50 kb from TSSs (Figure 4J). The Genomic Regions Enrichment of Annotations Tool (GREAT) identified meiosis and c-Myc pathways as the two leading pathways uniquely associated with $BAF155^{WT}$ but not $BAF155^{R1064K}$ (Figure 4K), implying that BAF155 methylation might direct its association with genes involved in potentially cancer-relevant c-Myc pathways.

BAF155 Methylation Controls Expression of Genes in the c-Myc Pathway

In contrast to the promoter regions of *CDH1* and *TFF1* genes where both $BAF155^{WT}$ and $BAF155^{R1064K}$ bind similarly (Figure S5A), many c-Myc pathway genes were selectively enriched for $BAF155^{WT}$ but not $BAF155^{R1064K}$, as shown in Figure S5B for *CDCA7*, *COL1A2*, *GADD45A*, *DDX18*, and *NDRG1* in HeLa and MCF7 cells. Next we performed conventional ChIP using distinct sets of biological samples to validate whether BAF155 is associated with the binding sites determined in the ChIP-seq experiment. As shown in

Figure 5A, BAF155^{WT} but not BAF155^{R1064K} was found associated with the ChIP-seq-implicated regions of *CDCA7*, *COL1A2*, *GADD45A*, *DDX18*, and *NDRG1*, whereas both BAF155 forms were detected at the promoter region of CDH1. ChIP using the me-BAF155 antibody confirmed the association of me-BAF155 to *COL1A2* and *GADD45A* genes in MCF7-BAF155^{WT} but not in MCF7-BAF155^{R1064K} cells (Figure 5B). Importantly, BAF155 association strongly correlated with gene expression. *COL1A2* and *GADD45A* mRNA levels, for example, were higher in MCF7-BAF155^{WT} than in MCF7-BAF155^{R1064} or MCF7-GFP with endogenous BAF155 silenced (Figure 5C). To examine whether the association of BAF155 with *COL1A2* and *GADD45A* genes depends on CARM1 expression, we performed ChIP assays in parental MCF7 and *CARM1* KO cells. As shown in Figures 5D and 5F, *CARM1* KO resulted in significant decreases of BAF155 association with the implicated regions of *COL1A2* and *GADD45A.* Thus, CARM1 is an important determinant for BAF155 genomic association, and CARM1-mediated BAF155 methylation could induce BAF155 association with unique genomic sites to control gene regulation. Interestingly, we could not detect binding above background of CARM1, BAF53, or SWI/SNF adenosine triphosphatase (ATPase) subunits BRG1 and BRM at the same regions of the *COL1A2* and *GADD45A* genes where BAF155 binds (Figures 5E and 5G), although BRG1 could be detected at positive control regions (e.g., the *CDH1* and *TFF1* promoters; Figures S5C and S5D). The positive binding of other SWI/SNF subunits SNF5, BAF53, and BRM to *CDH1* and *TFF1* genes similarly validated the corresponding antibodies for ChIP (Figure S5C). Despite the lack of detectable binding of BRG1 to *COL1A2*, *GADD45A*, and *NDRG1* regions (Figure S5D), SNF5 but not BAF53 was found at the BAF155-binding sites (Figures 5E, 5G, and S5D) of the corresponding genes. Accordingly, methylated BAF155 might be in a subcomplex with other BAFs such as SNF5 at unique chromatin sites.

BAF155 Methylation Correlates with Human Breast Cancer Progression and Malignancy

To determine whether me-BAF155 could serve as a prognostic biomarker for human breast cancer, we first optimized the me-BAF155 peptide antibody for immunohistochemistry (IHC). IHC staining of me-BAF155 could be completely blocked by me-BAF155 peptide but not by nonmethylated BAF155 peptide (Figure S6A), showing that the me-BAF155 antibody is specific. We next performed IHC using total BAF155 antibody as well as me-BAF155 antibody with four pairs of matched breast normal and tumor samples. As shown in Figure S6B, me-BAF155 staining was almost undetectable in normal samples, while both total BAF155 protein level and me-BAF155 intensity were elevated in breast tumors. Notably, CARM1 protein levels also were elevated in tumors relative to matched normal tissues (Figure S6C).

These results suggest that the increased level of me-BAF155 in tumors reflects overall elevated levels of BAF155 and CARM1. Thus, the me-BAF155 level might be a sensitive breast cancer progression biomarker. To test this hypothesis, we employed commercial tissue microarrays (TMAs), which contained ~80 samples from normal tissues, tumor-adjacent normal (TAN), benign tumors, malignant tumors, and metastatic tumors excised prior to treatment. Modest me-BAF155 staining was seen with normal (Figure 6A), TAN, and benign tissues (Figure 6B). In contrast, significantly greater me-BAF155 IHC staining was observed with malignant and metastatic tumors. One hundred percent of metastatic

tumors (6/6) showed strong positive staining for me-BAF155 (Figures 6C and 6D). To investigate if BAF155 methylation status is associated with clinical outcomes, we employed TMAs containing 372 breast tumor specimens with 150 months of clinical follow-up. TMAs were immunostained with me-BAF155-specific antibody, and specimens were rank ordered by immunostaining intensity and divided into me-BAF155-negative (bottom 25% intensity) and -positive (top 75% intensity) groups. The Kaplan-Meier plot shows that the me-BAF155-negative patients have a higher recurrence-free survival rate than do me-BAF155-positive patients (Figure 6E). A log-rank test performed to formally test this difference in recurrence-free survival rates yielded a statistically significant p value of 0.0497. Notably, the results of the multivariate analyses performed using the Cox proportional hazards model indicate a recurrence hazard 1.789 times higher for patients with me-BAF155-positive tumors when compared with me-BAF155-negative tumors ($p = 0.034$; Figures 6F and 6G). This hazard ratio of 1.789 for me-BAF155-positive tumors is similar to that of triple-negative breast cancer (hazard ratio = 1.845), a category well known for its poor prognosis. This difference in recurrence hazard rates is shown in the cumulative hazard plot (Figure 6F). These data underscored the potential use of me-BAF155 as a biomarker of malignant breast cancer and also in prognostic stratification of breast cancer patients.

Methylation of BAF155 Promotes Migration and Metastasis of Breast Cancer Cells In Vitro and In Vivo

To investigate of the role of BAF155 methylation in tumor migration and metastasis, we employed MDA-MB-231, an aggressive breast cancer cell line model, for in vitro transwell migration and in vivo metastasis studies. Using a strategy similar to that for MCF7 cells (Figure 4A), we engineered stable cell line MDA-MB-231-GFP with endogenous BAF155 knockdown, and its reconstituted derivatives MDA-MB-231-BAF155^{WT} and MDA-MB-231-BAF155^{R1064K} (Figure 7A). Knockdown of endogenous BAF155 in MDA-MB-231 cells significantly decreased cell growth (Figure 7B, compare ■ with □), which was rescued by restoring BAF155^{WT} but not BAF155^{R1064K} (Figure 7B, compare ▲ with Δ). Furthermore, knockdown of endogenous BAF155 in MDA-MB-231 cells significantly decreased cell migration in transwell assay, an effect that was partially rescued by restoring BAF155^{WT} but not BAF155^{R1064K} (Figure 7C). To explore the possibility that methylation of BAF155 is required for establishing metastatic lung colonization in vivo, we injected MDA-MB-231-BAF155^{WT} and MDA-MB-231-BAF155^{R1064K} cells stably expressing firefly luciferase intravenously to nude mice and monitored tumor cell colonization and outgrowth in lung using bioluminescence imaging. On the day of injection (day 0), both WT and mutant BAF155-expressing MDA-MB-231 cells accumulated in the lung as expected (Minn et al., 2005). Time-course analysis of the two cohorts revealed significant differences in lung colonization. BAF155^{WT}-expressing but not BAF155^{R1064K}-expressing cells showed colonization and tumor outgrowth in lung (Figure 7D). Thus, BAF155 methylation is positively linked to lung metastasis.

To gain further insight into the mechanism by which BAF155 methylation regulates MDA-MB-231 metastasis, we employed the tumor metastasis RT^2 profiler PCR array (SABiosciences), containing 84 genes involved in metastasis, to compare the mRNA expression profiles between MDA-MB-231-BAF155^{R1064K} and MDA-MB-231-BAF155^{WT}

(Figure 7E). If more than 2-fold expression difference was seen between the two cell lines, the corresponding genes are marked green or red (Figure 7E) and are listed in Figure 7F. Two metastasis repressor genes, *CDH11* and *KISS1R*, were upregulated, and six metastasis-promoting genes, *CCL7*, *CDH6*, *COL4A2*, *CXCL12*, *MMP13*, and *MYCL1*, were downregulated in MDA-MB-231-BAF155^{R1064K} cells compared with BAF155^{WT} cells. Four genes were selected for validation using real-time PCR. Indeed, *KISS1R* and *CDH11* were expressed at higher levels in MDA-MB-231-BAF155^{R1064K} cells, whereas *CCL7* and *COL4A2* were expressed at higher levels in MDA-MB-231-BAF155^{WT} cells (Figure 7G). We further systematically compared the differential gene expression of MDA-MB-231-BAF155^{WT} and -BAF155^{R1064K} using Affymetrix microarrays. Over 700 genes were differentially expressed in two cell lines ($p < 0.05$); 322 and 411 genes were upregulated and downregulated, respectively (Figure S7A). Among other differential expressed genes identified (Table S3), the metastasis genes *COL4A2* and *TIMP3* (Figure 7F) and c-MYC pathway gene *CDCA7* (Figure 5C) were expressed at higher levels in BAF155^{WT} cells than in BAF155^{R1064K} cells. Gene ontology pathway analyses revealed that the major differentially expressed genes fall in the categories of cellular movement, cellular organization, cell proliferation, and migration (Figure S7B). Moreover, despite the different cell lines used to study gene expression and DNA binding differences between WT BAF155 and BAF155^{R1064K}, one-fourth of the differentially expressed genes identified by microarrays in MDA-MB-231 cells overlap with differentially bound genomic regions identified by ChIP-seq in MCF7 cells (Figure S7C). These results suggest that BAF155 methylation regulates important pathways involved in cancer progression, including cell movement and migration.

Discussion

One important finding above is that knocking down endogenous CARM1 by 90% is insufficient to mimic the biological effects of complete *CARM1* KO. This echoes the in vivo mouse model where reducing *CARM1* to 25% of endogenous level still sustains normal development (Kim et al., 2010). Consistent with this, *CARM1* KO decreased cell and tumor growth in vitro and in vivo, in contrast to little in vivo growth effect of *CARM1* shRNA-mediated knockdown in MCF7 (Al-Dhaheri et al., 2011). While *CARM1* knockdown may selectively affect methylation of some substrates but not others, our findings underscore the importance of using complete KOs when studying the biological functions of enzymes.

Although engineered ZFNs have been used for genome editing in diverse model organisms, allele engineering in somatic cell genetics has not been widely applied for determining enzyme functions. KO efficiency by ZFNs varies among cancer cell lines and depends on transfection efficiency and the multiplicity of the targeted chromosome. For example, the *CARM1* disruption frequency reached 10% of alleles in diploid breast cancer cell line CAL51 (data not shown), compared with 1.3% in MCF7 cells where *CARM1*-bearing chromosome 19 is triplicated. In fact, one-time transient transfection of a plasmid encoding the *CARM1* ZFN in MCF7 cells only disrupted CARM1 biallelically, as confirmed by sequencing of genomic DNA. In agreement with a report that sequential ZFN transfection of biallelically disrupted clones resulted in triple locus KO at frequency of 1% (Liu et al., 2010), limiting dilution and genotyping without antibiotic selection yielded two MCF7

clones (out of 159) in which *CARM1* was disrupted triallelically (Figure 1E). Despite low KO frequency in some cases, ZFN-mediated KO of genes like *CARM1* in cancer cell lines provides unprecedented opportunities for cancer-relevant substrate discovery since, for example, MEFs lack or express many CARM1 substrates at lower level than *CARM1* null cancer cell lines. Identifying cancer-relevant substrates for CARM1 is essential for elucidating its functions in cancer, as exemplified by BAF155.

SWI/SNF is a multisubunit chromatin-remodeling complex that has been strongly implicated in cancer development due to aberrant expression and mutation of its subunits in many tumor types (Weissman and Knudsen, 2009). Accompanying the SWI/SNF ATPase subunits (e.g., BRG1) are 9–12 BAF proteins, including core and accessory subunits. The core subunits, BAF155, BAF170, and SNF5 (also referred to as SMARCB1, BAF47, or SNF5/INI1), were defined on the basis of their ability to restore efficient nucleosome remodeling in vitro (Phelan et al., 1999). Recent whole genome sequencing of human tumors revealed that SWI/SNF subunits are mutated in >20% of human malignancies (Kadoch et al., 2013). For example, SNF5 behaves as a bona fide tumor suppressor gene (Roberts et al., 2002). Conflicting evidence suggests that BAF155 may serve as tumor suppressor or oncogene in a tumor-type-specific manner. BAF155 was initially implicated as a tumor suppressor because of its residency in chromosome 3p21.31, a region frequently deleted in lung and other adenocarcinomas (Zabarovsky et al., 2002). Coincidently, BAF155 expression is deficient in two ovarian cancer cell lines, SKOV3 and SNUC2B (DelBove et al., 2011). However, mounting evidence supports that, for at least some tumor types, BAF155 might enhance tumor development. BAF155 expression is markedly induced in prostate cancer (Lapointe et al., 2004), cervical intraepithelial neoplasia (Shadeo et al., 2008), and colon cancer (Andersen et al., 2009). Elevated BAF155 expression was correlated with poor prognosis and recurrence in colon cancer (Andersen et al., 2009). The varied BAF155 expression in distinct tumor types suggests that aberrant BAF155 levels may contribute to tumor initiation and progression in a context-dependent manner.

We report here that BAF155 is elevated in human breast tumors and that increased methylation of BAF155 is associated with poor survival, implicating BAF155 as an independent prognosis biomarker. Individual ChIP experiments showed that some genomic sites seem to bind BAF155 independently of BRG1. Further ChIP-seq to improve signal/noise ratios and mapping of genomic sites using anti-me-BAF155 and BRG1 antibodies will more fully test BRG1-independent binding of BAF155 to chromatin sites. Nonetheless, our results support that methylated BAF155 might have functions independent from the full SWI/SNF complex, which agrees with earlier reports that individual SWI/SNF subunits confer oncogenic functions independently of the entire complex (Park et al., 2002). For example, BAF53 formed a distinct complex with c-Myc cofactors, including histone acetyltransferases to enhance c-Myc's oncogenic transformation activity (Park et al., 2002). It remains unknown whether me-BAF155 and SNF5 form complexes distinct from SWI/SNF at genomic loci specific for me-BAF155, including c-Myc pathway gene loci.

The c-Myc pathway deregulation is a common feature of human tumorigenesis. The Myc oncoprotein provides selective advantages to cancer cells by promoting proliferation, cell survival, genetic instability, and differentiation blockage, which all contribute to metastasis.

This study reveals that methylated BAF155 is specifically recruited to c-Myc pathway genes, some of which are direct c-Myc targets (e.g., *GADD45A*) and some of which are not (e.g., *COL1A2*). *COL1A2* produces a component of type I collagen, the pro-α2 (I) chain, involved in inflammatory response pathways. *COL1A2* was among a "meta-signature" associated with breast cancer prognosis (Urquidi and Goodison, 2007). *GADD45A* (DNA damage-inducible transcript 1 protein) functions as a stress sensor that modulates cellular responses to various stress conditions, including genotoxic and oncogenic stresses. Depending on the oncogenic stress, *GADD45A* could function as promoter or suppressor for breast cancer (Tront et al., 2010). *GADD45A* promotes tumor vascularization and growth of Myc-driven breast cancer via negative regulation of *MMP10* (Tront et al., 2010).

Recently, "poor prognosis" gene expression signatures in cancer, particularly in breast cancer, were found to reflect the activity of the c-Myc oncoprotein, which in turn regulates tumor metastasis through regulation of metastasis-relevant target genes and/or globally altering the epigenomic landscape of cancer cells (Wolfer et al., 2010). BAF155 methylation affects expression of a number of genes involved in metastasis. Interestingly, another study using the MDA-MB-231 cell line model showed that c-Myc knockdown had modest effects on primary tumor growth, whereas metastatic behavior and distant lung metastasis were greatly inhibited (Wolfer et al., 2010). This study suggests that c-Myc is essential for maintaining an invasive and migratory state of the highly metastatic MDA-MB-231 cells. Future studies will determine whether BAF155-methylation-sensitive metastatic genes are directly regulated by c-Myc. Given that 10%–15% of genomic loci in mammals are bound by c-Myc (Zeller et al., 2006), it is plausible that c-Myc affects metastasis-relevant gene expression via direct transcriptional regulation mechanism or via global alteration of chromatin structure of cancer cells, thus promoting the metastatic phenotype.

Experimental Procedures

Generation of CARM1 KO Cells

Cells were transiently transfected with plasmids encoding the indicated ZFN pairs using lipofectamine 2000 (Invitrogen) for 72 hr. Single-cell clones were isolated by limiting dilution of the ZFN-treated pool. The whole cell lysate of each clone was collected and CARM1 levels were detected by western blot. To analyze genomic DNA sequences of each positive clone, the target locus was first amplified by PCR using primers *CARM1*-ZFN-sense: 5′-ACAGCCTGCCTTCTCAGG-3′, anti-sense: 5′-TGCACAGCAATGGCAAGT-3′. Then the PCR product was cloned into pCR4-TOPO vector. For each cell line, plasmid DNAs from 50 bacterial colonies were sequenced.

Animal Models

All animal work was performed in accordance with protocols approved by Research Animal Resource Center of University of Wisconsin-Madison. Athymic nude mice at 5–6 weeks old were used for xenograft experiments (Harlan). Information for the animal experiments is presented in the Supplemental Experimental Procedures.

Human Primary Tumor Samples

Breast cancer TMAs constructed by UW Carbone Cancer Center include tumors from 372 individual subjects with Stage I to Stage III breast cancer treated at the UW Carbone Cancer Center from 1999to2007. The UW Health Sciences Institutional Review Board approved the TMA creation and waived institutional review board approval for future use of the TMA and coded data set.

In Vitro Methylation Assay

In vitro methylation assay was performed as previously described (Wang et al., 2013).

ChIP-seq Analysis

For experimental details, please refer to the Supplemental Experimental Procedures.

TMAs of Human Breast Tumors

TMAs constructed by UW Carbone Cancer Center include tumors from 372 individual subjects with Stage I to Stage III breast cancer treated from 1999 to 2007. The experimental details and statistical analyses are described in Supplemental Experimental Procedures.

Supplementary Material

Refer to Web version on PubMed Central for supplementary material.

Acknowledgments

We thank Dr. Charles Roberts for kindly providing the SNF5 antibody, Dr. Trevor K. Archer for BAF155 constructs, and Dr. Yin Zhang and Mark Horswill for valuable technical assistance with tail vein injection and DNA microarray experiments, respectively. This project was supported by a DOD ERA of HOPE Award (W81XWYH-11-1-0237 to W.X.) and National Institutes of Health grant CA22443 (to P.A.). P.A. is an investigator of the Howard Hughes Medical Institute and the Morgridge Institute for Research.

References

Al-Dhaheri M, Wu JC, Skliris GP, Li J, Higashimato K, Wang YD, White KP, Lambert P, Zhu YR, Murphy L, Xu W. CARM1 is an important determinant of ERα-dependent breast cancer cell differentiation and proliferation in breast cancer cells. Cancer Res. 2011; 71:2118–2128. [PubMed: 21282336]

Andersen CL, Christensen LL, Thorsen K, Schepeler T, Sørensen FB, Verspaget HW, Simon R, Kruhøffer M, Aaltonen LA, Laurberg S, Ørntoft TF. Dysregulation of the transcription factors SOX4, CBFB and SMARCC1 correlates with outcome of colorectal cancer. Br J Cancer. 2009; 100:511–523. [PubMed: 19156145]

Bedford MT, Clarke SG. Protein arginine methylation in mammals: who, what, and why. Mol Cell. 2009; 33:1–13. [PubMed: 19150423]

Chen J, Archer TK. Regulating SWI/SNF subunit levels via protein-protein interactions and proteasomal degradation: BAF155 and BAF170 limit expression of BAF57. Mol Cell Biol. 2005; 25:9016–9027. [PubMed: 16199878]

Chen D, Ma H, Hong H, Koh SS, Huang SM, Schurter BT, Aswad DW, Stallcup MR. Regulation of transcription by a protein methyltransferase. Science. 1999; 284:2174–2177. [PubMed: 10381882]

Cheng D, Côté J, Shaaban S, Bedford MT. The arginine methyltransferase CARM1 regulates the coupling of transcription and mRNA processing. Mol Cell. 2007; 25:71–83. [PubMed: 17218272]

Davis MB, Liu X, Wang S, Reeves J, Khramtsov A, Huo D, Olopade OI. Expression and sub-cellular localization of an epigenetic regulator, co-activator arginine methyltransferase 1 (CARM1), is associated with specific breast cancer subtypes and ethnicity. Mol Cancer. 2013; 12:40. [PubMed: 23663560]

DelBove J, Rosson G, Strobeck M, Chen JG, Archer TK, Wang WD, Knudsen ES, Weissman BE. Identification of a core member of the SWI/SNF complex, BAF155/SMARCC1, as a human tumor suppressor gene. Epigenetics. 2011; 6:1444–1453. [PubMed: 22139574]

Dhar S, Vemulapalli V, Patananan AN, Huang GL, Di Lorenzo A, Richard S, Comb MJ, Guo A, Clarke SG, Bedford MT. Loss of the major Type I arginine methyltransferase PRMT1 causes substrate scavenging by other PRMTs. Sci Rep. 2013; 3:1311. [PubMed: 23419748]

El Messaoudi S, Fabbrizio E, Rodriguez C, Chuchana P, Fauquier L, Cheng DH, Theillet C, Vandel L, Bedford MT, Sardet C. Coactivator-associated arginine methyltransferase 1 (CARM1) is a positive regulator of the Cyclin E1 gene. Proc Natl Acad Sci USA. 2006; 103:13351–13356. [PubMed: 16938873]

Euskirchen GM, Auerbach RK, Davidov E, Gianoulis TA, Zhong G, Rozowsky J, Bhardwaj N, Gerstein MB, Snyder M. Diverse roles and interactions of the SWI/SNF chromatin remodeling complex revealed using global approaches. PLoS Genet. 2011; 7:e1002008. [PubMed: 21408204]

Frietze S, Lupien M, Silver PA, Brown M. CARM1 regulates estrogen-stimulated breast cancer growth through up-regulation of E2F1. Cancer Res. 2008; 68:301–306. [PubMed: 18172323]

Kadoch C, Hargreaves DC, Hodges C, Elias L, Ho L, Ranish J, Crabtree GR. Proteomic and bioinformatic analysis of mammalian SWI/SNF complexes identifies extensive roles in human malignancy. Nat Genet. 2013; 45:592–601. [PubMed: 23644491]

Kim J, Lee J, Yadav N, Wu Q, Carter C, Richard S, Richie E, Bedford MT. Loss of CARM1 results in hypomethylation of thymocyte cyclic AMP-regulated phosphoprotein and deregulated early T cell development. J Biol Chem. 2004; 279:25339–25344. [PubMed: 15096520]

Kim D, Lee J, Cheng D, Li J, Carter C, Richie E, Bedford MT. Enzymatic activity is required for the in vivo functions of CARM1. J Biol Chem. 2010; 285:1147–1152. [PubMed: 19897492]

Lapointe J, Li C, Higgins JP, van de Rijn M, Bair E, Montgomery K, Ferrari M, Egevad L, Rayford W, Bergerheim U, et al. Gene expression profiling identifies clinically relevant subtypes of prostate cancer. Proc Natl Acad Sci USA. 2004; 101:811–816. [PubMed: 14711987]

Lee J, Bedford MT. PABP1 identified as an arginine methyltransferase substrate using high-density protein arrays. EMBO Rep. 2002; 3:268–273. [PubMed: 11850402]

Liu PQ, Chan EM, Cost GJ, Zhang L, Wang J, Miller JC, Guschin DY, Reik A, Holmes MC, Mott JE, et al. Generation of a triplegene knockout mammalian cell line using engineered zinc-finger nucleases. Biotechnol Bioeng. 2010; 106:97–105. [PubMed: 20047187]

Mann M, Cortez V, Vadlamudi R. PELP1 oncogenic functions involve CARM1 regulation. Carcinogenesis. 2013; 34:1468–1475. [PubMed: 23486015]

Minn AJ, Gupta GP, Siegel PM, Bos PD, Shu W, Giri DD, Viale A, Olshen AB, Gerald WL, Massagué J. Genes that mediate breast cancer metastasis to lung. Nature. 2005; 436:518–524. [PubMed: 16049480]

Park J, Wood MA, Cole MD. BAF53 forms distinct nuclear complexes and functions as a critical c-Myc-interacting nuclear cofactor for oncogenic transformation. Mol Cell Biol. 2002; 22:1307–1316. [PubMed: 11839798]

Phelan ML, Sif S, Narlikar GJ, Kingston RE. Reconstitution of a core chromatin remodeling complex from SWI/SNF subunits. Mol Cell. 1999; 3:247–253. [PubMed: 10078207]

Roberts CWM, Leroux MM, Fleming MD, Orkin SH. Highly penetrant, rapid tumorigenesis through conditional inversion of the tumor suppressor gene Snf5. Cancer Cell. 2002; 2:415–425. [PubMed: 12450796]

Shadeo A, Chari R, Lonergan KM, Pusic A, Miller D, Ehlen T, Van Niekerk D, Matisic J, Richards-Kortum R, Follen M, et al. Up regulation in gene expression of chromatin remodelling factors in cervical intraepithelial neoplasia. BMC Genomics. 2008; 9:64. [PubMed: 18248679]

Shi SP, Qiu JD, Sun XY, Suo SB, Huang SY, Liang RP. PMeS: prediction of methylation sites based on enhanced feature encoding scheme. PLoS ONE. 2012; 7:e38772. [PubMed: 22719939]

Tomlins SA, Mehra R, Rhodes DR, Cao X, Wang L, Dhanasekaran SM, Kalyana-Sundaram S, Wei JT, Rubin MA, Pienta KJ, et al. Integrative molecular concept modeling of prostate cancer progression. Nat Genet. 2007; 39:41–51. [PubMed: 17173048]

Tront JS, Huang Y, Fornace AJ Jr, Hoffman B, Liebermann DA. Gadd45a functions as a promoter or suppressor of breast cancer dependent on the oncogenic stress. Cancer Res. 2010; 70:9671–9681. [PubMed: 21098706]

Urquidi V, Goodison S. Genomic signatures of breast cancer metastasis. Cytogenet Genome Res. 2007; 118:116–129. [PubMed: 18000362]

Varambally S, Yu J, Laxman B, Rhodes DR, Mehra R, Tomlins SA, Shah RB, Chandran U, Monzon FA, Becich MJ, et al. Integrative genomic and proteomic analysis of prostate cancer reveals signatures of metastatic progression. Cancer Cell. 2005; 8:393–406. [PubMed: 16286247]

Wang L, Charoensuksai P, Watson NJ, Wang X, Zhao Z, Coriano CG, Kerr LR, Xu W. CARM1 automethylation is controlled at the level of alternative splicing. Nucleic Acids Res. 2013; 41:6870–6880. [PubMed: 23723242]

Weissman B, Knudsen KE. Hijacking the chromatin remodeling machinery: impact of SWI/SNF perturbations in cancer. Cancer Res. 2009; 69:8223–8230. [PubMed: 19843852]

Wolfer A, Wittner BS, Irimia D, Flavin RJ, Lupien M, Gunawardane RN, Meyer CA, Lightcap ES, Tamayo P, Mesirov JP, et al. MYC regulation of a “poor-prognosis” metastatic cancer cell state. Proc Natl Acad Sci USA. 2010; 107:3698–3703. [PubMed: 20133671]

Wu J, Xu W. Histone H3R17me2a mark recruits human RNA polymerase-associated factor 1 complex to activate transcription. Proc Natl Acad Sci USA. 2012; 109:5675–5680. [PubMed: 22451921]

Yadav N, Lee J, Kim J, Shen J, Hu MC, Aldaz CM, Bedford MT. Specific protein methylation defects and gene expression perturbations in coactivator-associated arginine methyltransferase 1-deficient mice. Proc Natl Acad Sci USA. 2003; 100:6464–6468. [PubMed: 12756295]

Zabarovsky ER, Lerman MI, Minna JD. Tumor suppressor genes on chromosome 3p involved in the pathogenesis of lung and other cancers. Oncogene. 2002; 21:6915–6935. [PubMed: 12362274]

Zeller KI, Zhao X, Lee CW, Chiu KP, Yao F, Yustein JT, Ooi HS, Orlov YL, Shahab A, Yong HC, et al. Global mapping of c-Myc binding sites and target gene networks in human B cells. Proc Natl Acad Sci USA. 2006; 103:17834–17839. [PubMed: 17093053]

Zeng H, Wu J, Bedford MT, Sbardella G, Hoffmann FM, Bi K, Xu W. A TR-FRET-based functional assay for screening activators of CARM1. ChemBioChem. 2013; 14:827–835. [PubMed: 23585185]

Significance

Although mutations or epigenetic changes inactivating and altering the functions of chromatin remodeling complex SWI/SNF are frequently linked to cancer, the mechanisms underlying these connections remain unclear. Delineating the factors and pathways that induce SWI/SNF's oncogenic effects would enable preventive and therapeutic targeting of these cancer-driving changes while retaining SWI/SNF's normal functions. Here, we identify BAF155, a SWI/SNF core subunit, as a substrate for arginine methyltransferase CARM1. Methylation of BAF155 is required for its association with genomic sites that drive regulation of genes in the c-Myc and certain metastatic pathways. This represents a mechanism by which a chromatin-remodeling factor is activated by arginine methylation to regulate genes that enhance tumor progression and metastasis.

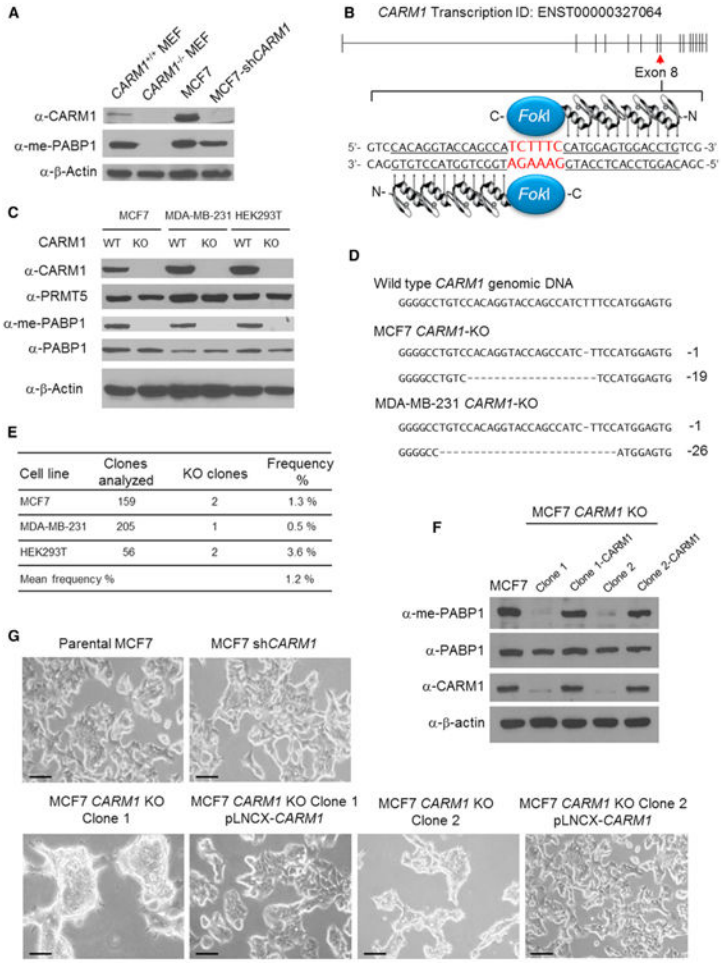

Figure 1. Generation of CARM1 KO Breast Cancer Cell Lines

(A) Western blot analysis of CARM1 and methyl-PABP1 using whole cell lysates from *CARM1*$^{+/+}$ MEF, *CARM1*$^{-/-}$ MEF, MCF7, and MCF7-sh*CARM1* cells. β-Actin was used as a loading control.

(B) Targeting exon 8 of human *CARM1* by ZFN.

(C) Western blot of CARM1, PABP1, methyl-PABP1, PRMT5 in parental and *CARM1* KO MCF7, MDA-MB-231, and HEK293T cells.

(D) Genomic DNA sequence of ZFN targeting site in MCF7 *CARM1* KO and MDA-MB-231 *CARM1* KO cell clones.

(E) ZFN-mediated KO frequency of CARM1 in each indicated cell line.

(F) Western blot of CARM1, PABP1, and me-PABP1 in MCF7, two MCF7 *CARM1* KO clones, and MCF7 *CARM1* KO clones re-expressing CARM1 by retroviral infection.

(G) Representative cell morphology images of MCF7 cells, MCF7-sh*CARM1* cells, and the MCF7-derived *CARM1* KO cell lines listed in (F). Scale bar = 40 μm.

See also Figure S1.

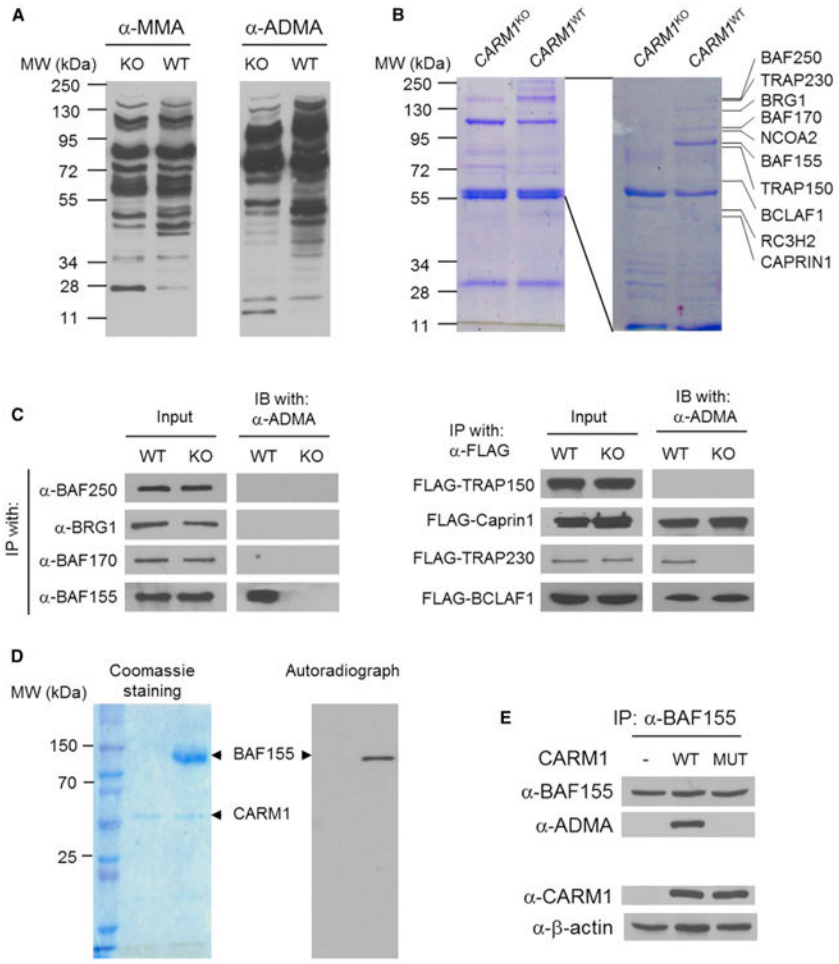

Figure 2. Identification of BAF155 as a Substrate for CARM1

(A) Western blot analysis of total proteins in MCF7 and MCF7 *CARM1* KO cells using antibodies against MMA and ADMA moieties.

(B) Coomassie brilliant blue staining of proteins immunoprecipitated with anti-ADMA antibody from total cell lysates of MCF7 and MCF7 *CARM1* KO cells. Discrete bands in the high molecular weight range were excised and subjected to mass spectrometry analysis, from which ten candidate proteins were identified (right panel).

(C) Western blot analysis of input and anti-ADMA immunoprecipitated proteins using antibodies to detect endogenous BRG1, BAF170, BAF155, and BAF250, or against the FLAG epitope to detect transfected, FLAG-tagged TRAP150, Caprin1, TRAP230, and BCLAF1 in HEK293T and HEK293T *CARM1* KO cells.

(D) Coomassie brilliant blue staining (left panel) and autoradiograph (right panel) of in vitro methylated BAF155 by CARM1 in the presence of ^{3}H-SAM.

(E) Western blot analysis of anti-BAF155 immunoprecipitated proteins using anti-ADMA, BAF155, and CARM1 antibodies in HEK293T CARM1 KO cells before and after restoration with WT CARM1 or a methylation-defective CARM1 mutant (MUT).

See also Figure S2.

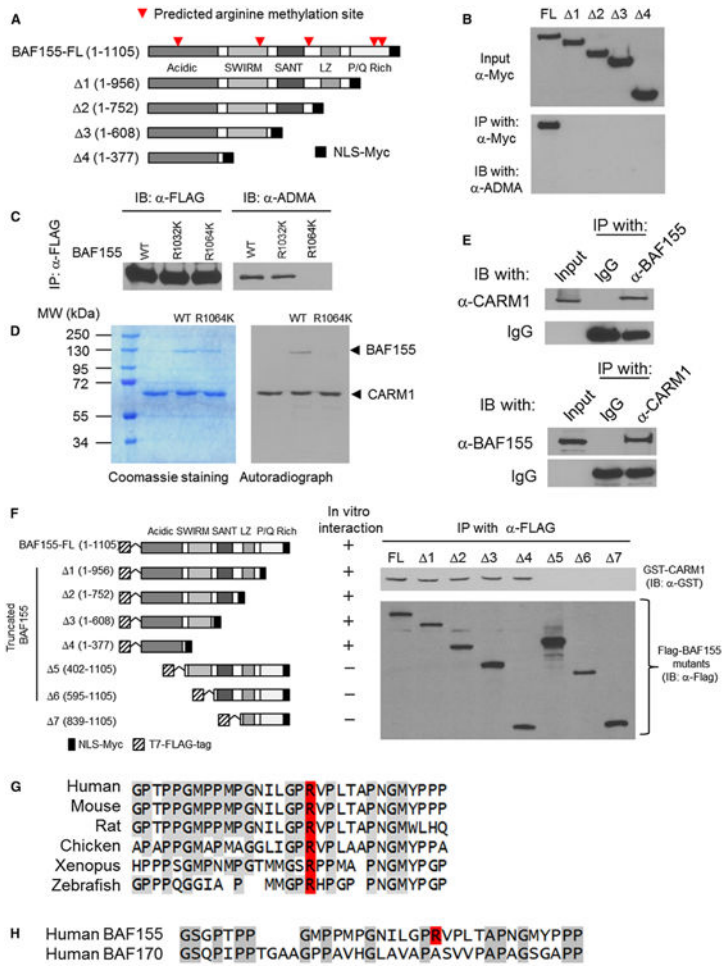

Figure 3. CARM1 Methylates BAF155 at a Single Site, R1064

(A) Schematic diagram of BAF155 full-length cDNA and C-terminally truncated derivatives, each with a nuclear localization sequence/Myc (NLS-Myc) epitope tag cassette fused to its C terminus. Red arrows point to putative arginine methylation sites predicted by the PMeS program.

(B) Plasmids expressing the BAF155 cDNA derivatives shown in (A) were transiently transfected into HEK293 cells and detected by western blotting with anti-Myc antibody (upper panel). Total cell lysates were immunoprecipitated with anti-Myc antibody and western blotted with anti-ADMA antibody (lower panel).

(C) FLAG-tagged recombinant $BAF155^{WT}$, $BAF155^{R1032K}$, and $BAF155^{R1064K}$ proteins were immunoprecipitated from HEK293T cells with anti-FLAG antibody and detected by western blotting using anti-FLAG (left panel) or anti-ADMA (right panel) antibodies.

(D) In vitro assay using recombinant CARM1 and ^{3}H-SAM to test for methylation of $BAF155^{WT}$ and $BAF155^{R1064K}$ proteins prepared from HEK293T *CARM1* KO cells.

(E) Reciprocal coimmunoprecipitation of CARM1 with BAF155, and BAF155 with CARM1, from MCF7 cell lysates.

(F) Mapping of CARM1-interacting domain to the N-terminal acidic domain of BAF155 by GST-pull-down assay. Left panel shows schematic diagrams of FLAG-tagged BAF155 truncation derivatives that were incubated with GST-CARM1 proteins and immunoprecipitated with anti-FLAG antibody. The immunoprecipitates were tested for the presence of GST-CARM1 by western blotting using anti-GST antibody (right panel).

(G) CLUSTALW alignment of vertebral BAF155 sequences flanking human BAF155 methylation site R1064, which is highlighted in red.

(H) CLUSTALW alignment of P/Q-rich domain sequences of BAF155 (with R1064 highlighted in red) and its homolog BAF170 protein.

See also Figure S3 and Table S1.

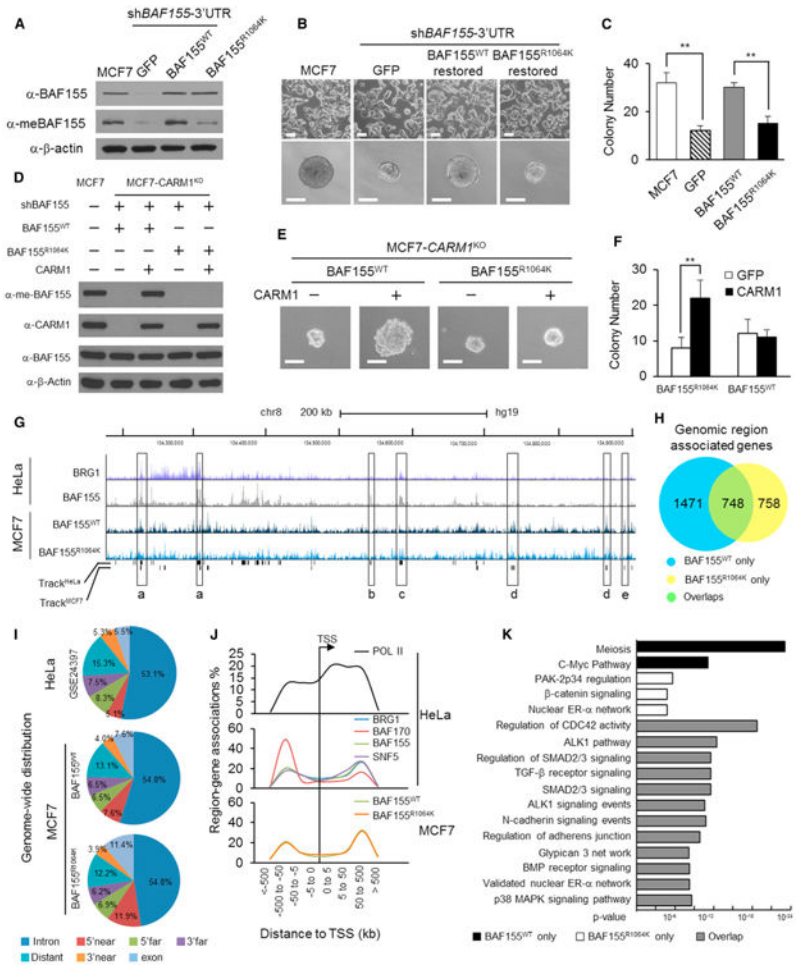

Figure 4. BAF155 Methylation Promotes MCF7 Cell Colony Formation and Directs Unique Genomic Association Patterns

(A) Western blotting of BAF155 and me-BAF155 in MCF7 cells and MCF7-sh*BAF155* cells restored with GFP, BAF155^{WT}, or BAF155^{R1064K}.

(B) Representative images of cell morphology (upper panel; scale bars = 40 μm) and colonies (lower panel; scale bars = 100 μm) for parental MCF7 and MCF7-sh*BAF155*-GFP cells, and BAF155^{WT}- and BAF155^{R1064K}-restored MCF7 cells.

(C) Colony yields for the cell lines in (B).

(D) Western blotting analysis of CARM1, BAF155, and me-BAF155 proteins in MCF7 *CARM1* KO clone 1, MCF7-*CARM1*KO-BAF155^{WT}, and MCF7-*CARM1*KO-BAF155^{R1064K} cells engineered to express either GFP or CARM1. β-Actin was used as loading control.

(E) Representative images of colonies formed by each cell line shown in (D). Scale bar = 100 mm.

(F) Colony yields for the cell lines in (D).

(G) ChIP-seq identifies BRG1, BAF155^{WT}, and BAF155^{R1064K} association in an ~750 kb region of chromosome 8. The coordinates shown are in hg19 and all regions were identified in MCF7and HeLa cells as detailed in Table S2. An “a” denotes a peak that is detected by BRG1 and BAF155 in both HeLa and MCF7; “b” denotes BAF155 binding peak only found in HeLa cells; “c” denotes shared BAF155and BRG1 binding peaks in HeLa but not in MCF7 cells; “d” denotes shared BAF155^{WT} and BAF155^{R1064K} peaks only found in MCF7 cells; and “e” denotes BAF155^{WT} binding only found in MCF7 cells.

(H) Venn diagram showing the overlapping and discrete BAF155cistromes in MCF7 cells expressing BAF155^{WT}and BAF155^{R1064K}. Genomic-region-associated genes were defined as the regions between 5.0 kb upstream and 1.0 kb downstream of annotated genes, using GREAT.

(I) Distribution of the genome-wide association of BAF155 binding sites in MCF7 cells is comparable to that in HeLa cells.

(J) Distribution of genomic association sites of RNA pol II and SWI/SNF subunits relative to TSSs in HeLa (top two panels) and MCF7 cells (bottom panel).

(K) BAF155 genomic association sites map to different signaling pathways in MCF7-BAF155^{WT} and MCF7-BAF155^{R1064K} cells.

Quantitative data are presented as averages ± SD. Student's t test was used for statistical analysis. **$p < 0.01$. See also Figure S4 and Table S2.

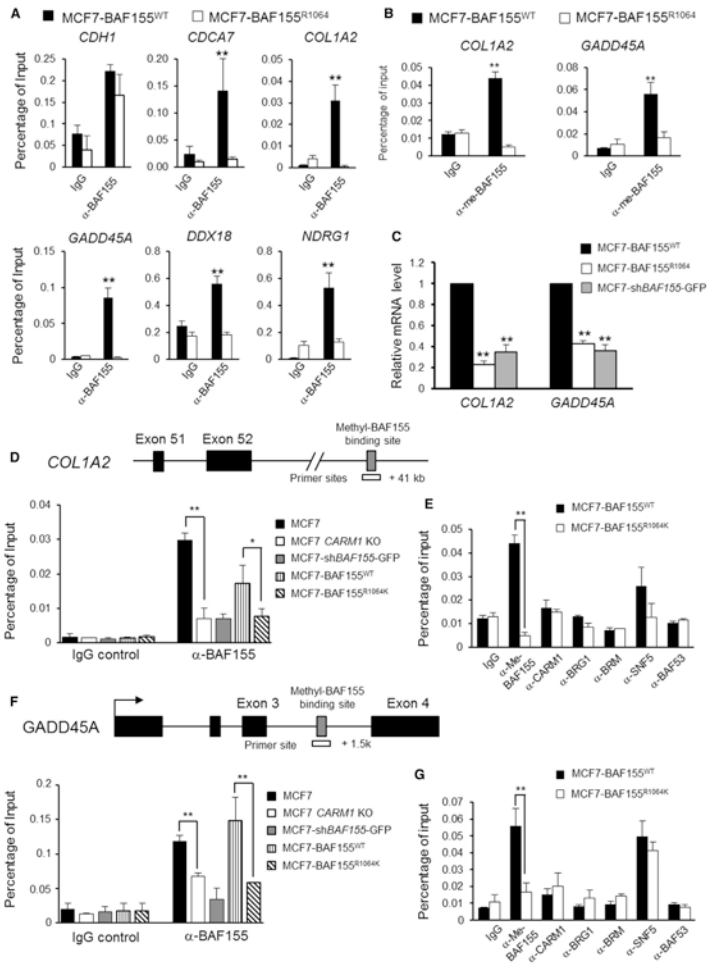

Figure 5. BAF155 Methylation Controls Expression of Genes in the c-Myc Pathway

(A) Differential binding of BAF155 to *CDCA7*, *COL1A2*, *GADD45A*, *DDX18*, and *NDRG1* genes was analyzed using ChIP-quantitative PCR (qPCR) in MCF7-BAF155^{WT} and MCF7-BAF155^{R1064K} cells. BAF155^{WT} and BAF155^{R1064K} displayed similar binding to the positive control CDH1 gene. Normal rabbit immunoglobulin G (IgG) was used as antibody control.

(B) ChIP-qPCR analysis of me-BAF155 binding to *COL1A2* and *GADD45A* genes.

(C) Relative mRNA levels of *COL1A2* and *GADD45A* in MCF7-sh*BAF155*, MCF7-BAF155^{WT}, and MCF7-BAF155^{R1064K} cells were determined by real-time qPCR. β-Actin was used as an internal control.

(D) The me-BAF155 binding region on the *COL1A2* gene and ChIP-qPCR analysis of BAF155 association with the *COL1A2* gene in MCF7, MCF7 *CARM1* KO, MCF7-sh*BAF155*-GFP, MCF7-BAF155^{WT}, and MCF7-BAF155R^{1064K} cells.

(E) ChIP-qPCR analysis of me-BAF155, CARM1, BRG1, BRM, BAF53, and SNF5 association with the *COL1A2* gene in MCF7-BAF155^{WT} and MCF7-BAF155^{R1064K} cells. Normal rabbit IgG was used as control.

(F) ChIP-qPCR analysis of me-BAF155 association with the *GADD45A* gene in the indicated cells.

(G) ChIP-qPCR analysis of the association of me-BAF155, CARM1, BRG1, BRM, BAF53, and SNF5 with the *GADD45A* gene in MCF7-BAF155^{WT} and MCF7-BAF155^{R1064K} cells.

Quantitative data are presented as averages ± SD. Student's t test was used for statistical analysis. **p < 0.01. See also Figure S5.

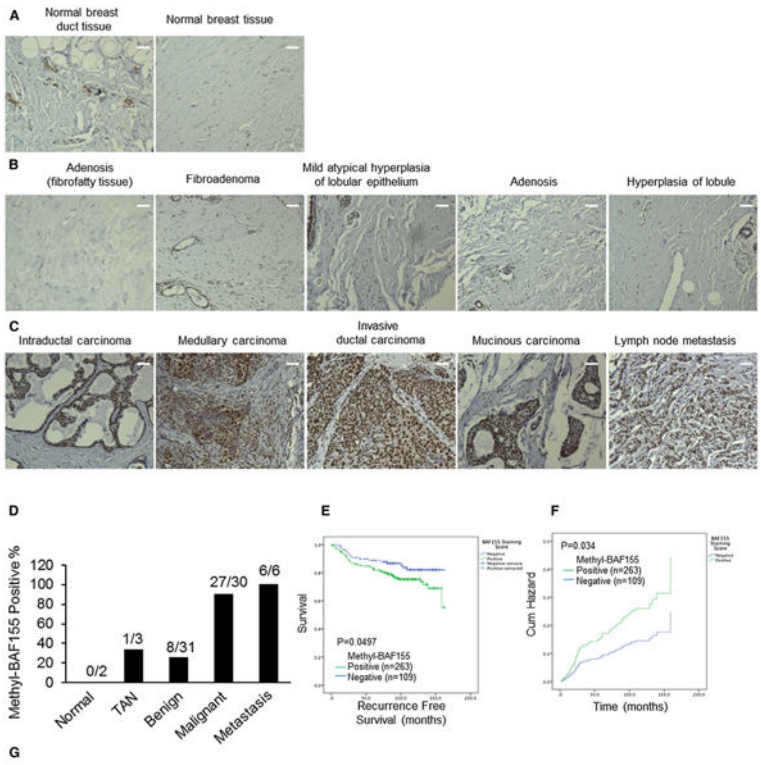

G

ANOVA table for cancer recurrence

Parameter		Parameter Estimate	Standard Error	Chi-Square	P-value	Hazard Ratio
Stage	II	1.182	0.307	14.845	0.000	3.260
Stage	III	1.850	0.360	26.402	<0.001	6.357
Triple Negative Status	NEG	0.613	0.330	3.444	0.064	1.845
BAF155 intensity	POS	0.582	0.275	4.481	0.034	1.789

Figure 6. BAF155 Methylation Correlates with Human Breast Cancer Progression, Malignancy, and Recurrence-Free Survival

(A–C) Immunohistochemical staining of me-BAF155 in representative normal breast (A), benign breast tumors (B), and malignant breast tumors including lymph node metastasis specimens (C) on the US Biomax BR723 TMA. Brown staining denotes me-BAF155 immunoreactivity. Scale bar = 200 μm.

(D) The percentage of me-BAF155-positive staining in normal, TAN, benign, malignant, and metastatic samples on the BR723 TMA.

(E) Kaplan-Meier curves depicting the probability of recurrence-free survival in breast cancer patients stratified by me-BAF155 IHC positivity in primary tumors.

(F) Kaplan-Meier curves for cumulative hazard (Cum Hazard).

(G) The recurrence hazard for breast cancer patients stratified by me-BAF155 staining positivity using a Cox proportional hazards model.

See also Figure S6.

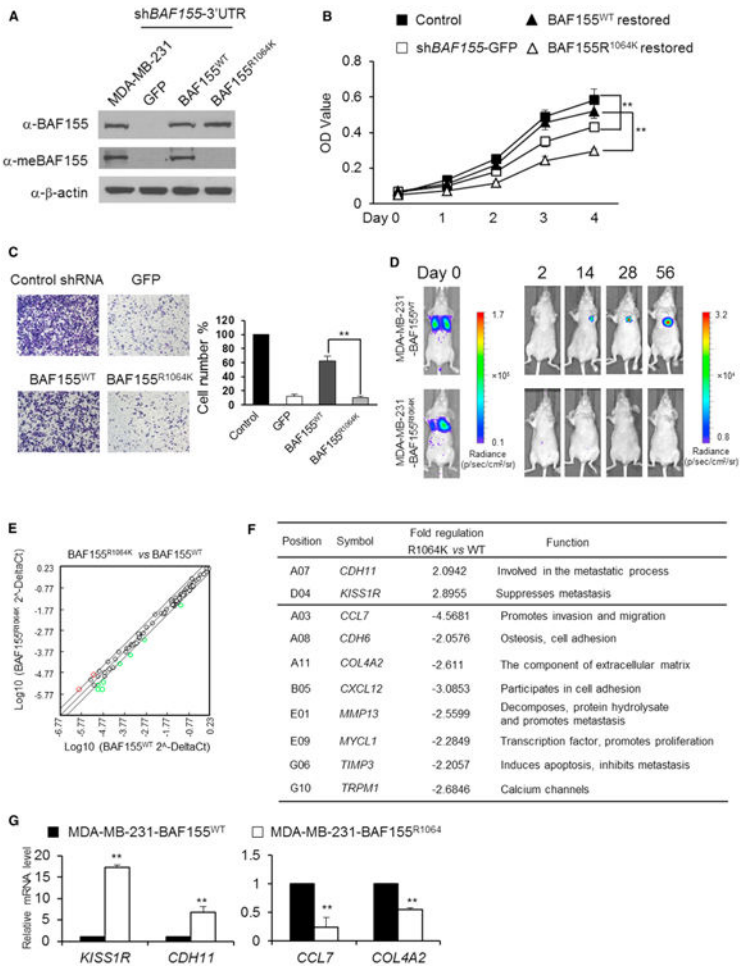

Position	Symbol	Fold regulation R1064K *vs* WT	Function
A07	*CDH11*	2.0942	Involved in the metastatic process
D04	*KISS1R*	2.8955	Suppresses metastasis
A03	*CCL7*	-4.5681	Promotes invasion and migration
A08	*CDH6*	-2.0576	Osteosis, cell adhesion
A11	*COL4A2*	-2.611	The component of extracellular matrix
B05	*CXCL12*	-3.0853	Participates in cell adhesion
E01	*MMP13*	-2.5599	Decomposes, protein hydrolysate and promotes metastasis
E09	*MYCL1*	-2.2849	Transcription factor, promotes proliferation
G06	*TIMP3*	-2.2057	Induces apoptosis, inhibits metastasis
G10	*TRPM1*	-2.6846	Calcium channels

Figure 7. BAF155 Methylation Promotes Breast Cancer Cell Migration and Metastasis In Vitro and In Vivo

(A) Generation of an MDA-MB-231 cell derivative with endogenous BAF155 silenced and further derivatives with $BAF155^{WT}$or $BAF155^{R1064K}$expression restored in this MDA-MB-231-sh*BAF155* cell background. Total BAF155 and me-BAF155 were detected with corresponding antibodies by western blotting.

(B) The (3-[4,5-dimethylthiazol-2-yl]-2,5 diphenyl tetrazolium bromide assays of MDA-MB-231 cells and MDA-MB-231-sh*BAF155* cells expressing GFP, $BAF155^{WT}$, or $BAF155^{R1064K}$.

(C) Transwell assays measuring the migration ability of cell lines in (B).

(D) Bioluminescence images of colonized and metastatic MDA-MB-231-sh*BAF155* cells stably expressing firefly luciferase and $BAF155^{WT}$ or $BAF155^{R1064K}$ in nude mice at the indicated times following tumor introduction through tail vein injection (n = 5). Representative images are shown from each cohort.

(E) Scatter plot of mRNA levels for 84 metastasis-implicated genes analyzed by the tumor metastasis RT^2 profiler PCR array (SABiosciences); red and green circles mark genes that are differentially expressed ≥2-fold between MDA-MB-231-sh*BAF155* cells restored with $BAF155^{WT}$ or $BAF155^{R1064K}$.

(F) List of >2-fold differentially expressed genes in (E). Positive fold change represents overexpression in $BAF155^{R1064K}$ cells.

(G) Real-time qPCR analyses of *KISS1R*, *CDH11*, *CCL7*,and *COL4A2* mRNA levels in MDA-MB-231-sh*BAF155* cells restored with $BAF155^{WT}$and $BAF155^{R1064K}$. β-Actin was used as an internal control.

See also Figure S7 and Table S3.